# Electronic Spin Storage in an Electrically Readable Nuclear Spin Memory with a Lifetime >100 Seconds

D. R. McCamey,[1]*† J. Van Tol,[2] G. W. Morley,[3] C. Boehme[1]

Electron spins are strong candidates with which to implement spintronics because they are both mobile and able to be manipulated. The relatively short lifetimes of electron spins, however, present a problem for the long-term storage of spin information. We demonstrated an ensemble nuclear spin memory in phosphorous-doped silicon, which can be read out electrically and has a lifetime exceeding 100 seconds. The electronic spin information can be mapped onto and stored in the nuclear spin of the phosphorus donors, and the nuclear spins can then be repetitively read out electrically for time periods that exceed the electron spin lifetime. We discuss how this memory can be used in conjunction with other silicon spintronic devices.

The ability to store and retrieve spin information in solid-state systems is important for the development of spin-based electronic devices for classical and quantum information processing. The ability to store spin information in situ enhances the ability to integrate spintronic and classical electronic systems, allows the stored spin to be used as an initialized classical or quantum register, and may provide the ability to perform quantum nondemolition readout on difficult-to-probe spin systems. Nuclear spins are an obvious candidate for implementing such a memory, because they tend to have extremely long spin lifetimes (*1*–*3*).

To date, implementations of quantum logic or memory devices directly involving nuclear spins have used optical or microwave detection in systems such as the nitrogen vacancy center of diamond (*4*–*6*). However, coupling these systems to classical electronic devices requires transduction between optical and electrical signals. We demonstrated electrical readout of a nuclear spin memory consisting of phosphorus donors in silicon. Previous work to electrically detect nuclear spin states has focused on continuous-wave spin resonance techniques, which are unsuitable for the manipulation required for nuclear spin storage (*7*), and on electrically detected nuclear magnetic resonance approaches using quantum Hall edge states in gallium arsenide heterostructures (*8*).

Phosphorus donors in silicon (Si:P) provide a number of advantages for the implementation of such a device. Si:P is widely used in the modern semiconductor industry, providing the ability to fabricate devices on the scale of a few nanometers (*9*). Recent work has demonstrated that $^{31}$P-doped silicon can be used for spintronic applications (*10*), allowing long-distance spin transport with conduction electrons (*11*). Additionally, the phosphorus donor has long electron (*12*) and extremely long nuclear spin (*3*) coherence times, making it an ideal system for implementing such a device.

As a result of these properties, Si:P has been widely investigated for use in applications ranging from quantum information processing (*2*, *13*, *14*) to more "classical" spintronics (*10*, *11*), where the phase of the spin is less important. However, few advances related to the nuclear spin of donors have been reported (*2*, *15*–*17*). It has been demonstrated that an ensemble of coherent donor electron spin states could be stored in the nuclear spin for over a second, before being returned to the electrons and read out with conventional spin resonance techniques (*2*). Recently, it was also shown that the spin state of a single electron in silicon could be detected electrically with a single shot, although simultaneous control of the spin has yet to be demonstrated (*14*).

Previous attempts to use electrical spin readout of donors with the pulsed manipulation of their nuclear spins required for storage have proven challenging because of the small characteristic change in current seen at low magnetic fields. By using high magnetic fields (~8.59 T), we are able to obtain large electron spin polarization and a correspondingly large change in current (*18*). The difficulty with these large fields is that the frequencies required for electron spin manipulation are ~240 GHz. The recent development of pulsed spin resonance at these frequencies allows these measurements to be performed.

In high magnetic fields, the product states of the $^{31}$P donor electron and nuclear spin system, $|\uparrow_e \uparrow_n\rangle$, $|\downarrow_e \uparrow_n\rangle$, $|\uparrow_e \downarrow_n\rangle$, and $|\downarrow_e \downarrow_n\rangle$ are very close to the eigenstates (↑ and ↓ represent the individual spin-up and spin-down eigenstates, respectively). Allowed transitions between these

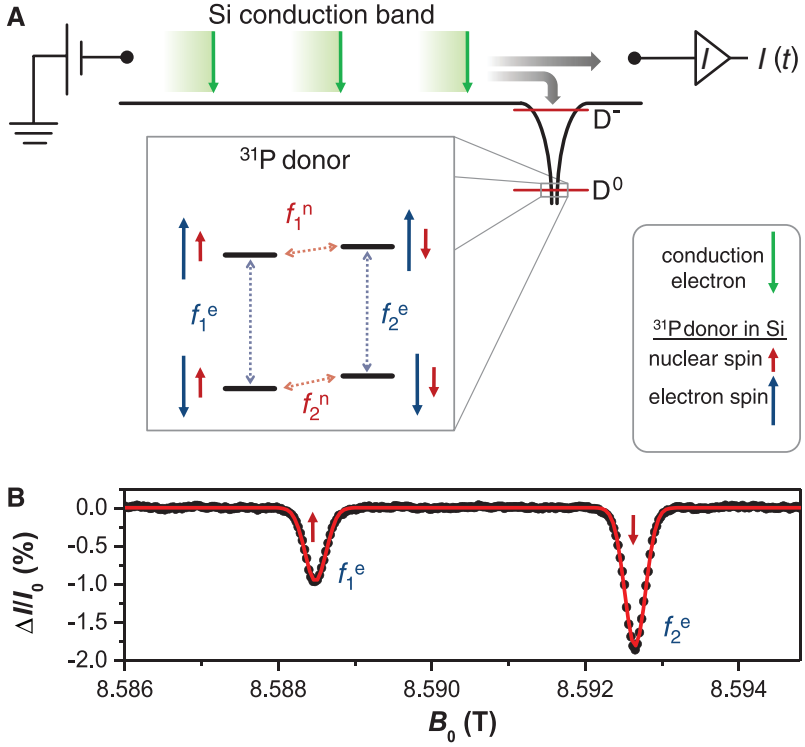


**Fig. 1.** The Si:P system used for implementing spin storage. (**A**) The singly occupied ($D^0$) state of the phosphorus donor in silicon may capture a conduction electron and form a doubly occupied ($D^-$) state only if they have opposite spin. Modifying the capture rate by manipulating the donor electron spin leads to a change in current through the silicon crystal. (**B**) Electron spin resonance reveals two resonances in the device current, due to the different donor nuclear-spin orientations, which couple to the electron spins through a contact hyperfine interaction.

[1]Department of Physics and Astronomy, University of Utah, Salt Lake City, UT, 84112, USA. [2]National High Magnetic Field Laboratory, Florida State University, Tallahassee, FL 32310, USA. [3]London Centre for Nanotechnology and Department of Physics and Astronomy, University College London, London WC1H 0AH, UK.

*Present address: School of Physics, University of Sydney, Sydney 2006, Australia.

†To whom correspondence should be addressed. E-mail: dane.mccamey@sydney.edu.au

states can be driven by spin resonance (Fig. 1A). The presence of a contact hyperfine interaction of 117.5 MHz between the electron and nucleus, along with the nonnegligible nuclear Zeeman energy (148.2 MHz at 8.59 T), lifts the degeneracy of the spin resonance conditions, allowing the four transitions to be independently addressed. We use a custom built 240 GHz pulsed spectrometer (*19*–*21*) to drive these transitions, at a temperature ($T$) = 3.5 ± 0.2 K. To read out the nuclear spin state, we use a spin trap method (*18*): If the conduction electrons are polarized in the spin-down state, the doubly occupied $D^-$ state of the donor cannot be occupied if the donor electron also has spin down. However, if the donor electron is resonantly excited to the spin-up state, then the $D^-$ state is able to trap an electron from the conduction band, thus reducing the conductivity of the silicon. This can be detected by measuring the change in the conductivity after resonant excitation, using the circuit

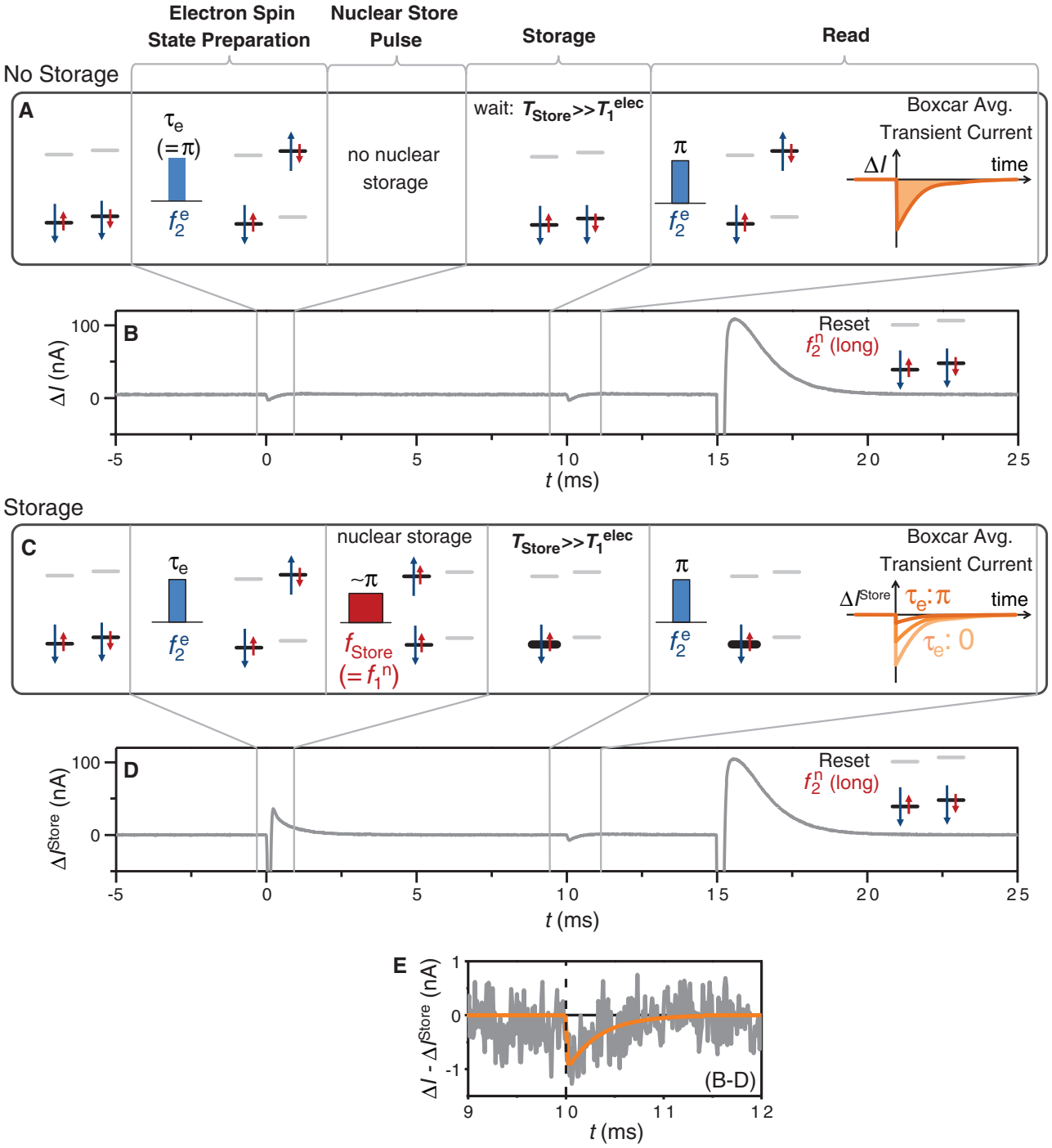


**Fig. 2.** Schematic of different storage pulse sequences. (**A**) The electron is prepared into a 1 state by applying a $\pi(f_2^e)$ pulse. If no nuclear spin storage is undertaken, the initial spin state has no impact on the final spin state obtained. (**B**) Transient current during the pulse sequence in (A). (**C**) However, if the electron is prepared into a 1 state then stored in the nuclear spin, the magnitude of the current change after the readout pulse is reduced. (**D**) The change in the current through the silicon sample during the application of a STORE-1 sequence. The large nonresonant current changes at 0 and 15 ms are due to nonresonant coupling of the radio frequency (rf) to the electrical contacts. (**E**) Difference between NO STORE and STORE transient current for the initial state 1. The solid orange line is a fit to the data for time ($t$) > 10 ms.

shown in Fig. 1A. Figure 1B shows the change in current after a 240-GHz π pulse was applied to the device as the external magnetic field $B_0$ was varied, bringing the $f_1^e$ and $f_2^e$ transitions on resonance at 8.5885 and 8.5927 T, respectively. The difference in amplitude is due to an Overhauser-mediated nuclear polarization effect (*15*) and is not important to the nuclear storage.

A nuclear storage and electrical readout experiment was performed using a modified Davies electron-nuclear double resonance (ENDOR) scheme (*22*–*24*), previously only demonstrated on a sample containing a large number of donors (>4 × $10^{12}$) in a conventional ENDOR approach. Because of the large electron spin polarization, the initial state of the phosphorus donors is $|\downarrow_e \uparrow_n\rangle$ or $|\downarrow_e \downarrow_n\rangle$. In the experiments, P atoms in the $|\downarrow_e \uparrow_n\rangle$ state remain unchanged while those in the $|\downarrow_e \downarrow_n\rangle$ state are used for storage. If a pure initial state is required, the pulse sequence $[\pi(f_1^e) - \pi(f_2^n) -$ wait $> T_1^e]$ maps $|\downarrow_e \uparrow_n\rangle$ onto $|\downarrow_e \downarrow_n\rangle$ while leaving those donors initially in $|\downarrow_e \downarrow_n\rangle$ in that state. We prepared some arbitrary electronic spin state $|\downarrow_e \downarrow_n\rangle \xrightarrow{\tau_e(f_2^e)} \alpha|\downarrow_e \downarrow_n\rangle + \beta|\uparrow_e \downarrow_n\rangle$ by applying a $\tau_e(f_2^e)$ pulse of varying length (Fig. 2, A and C). Logical information can thus be encoded in the electron spins: Ensembles comprising spins in the spin-up eigenstates are assigned as "1" and in the spin-down eigenstate as "0".

The ensemble electron spin state can now be stored in a nuclear spin state by applying a controlled NOT (CNOT) gate [a $\pi(f_1^n)$ pulse] between the electronic and nuclear spin (Fig. 2C): $\alpha|\downarrow_e \downarrow_n\rangle + \beta|\uparrow_e \downarrow_n\rangle \xrightarrow{\pi(f_1^n)} \alpha|\downarrow_e \downarrow_n\rangle + \beta|\uparrow_e \uparrow_n\rangle$.

The nuclear spin state can then be read at later times by measuring the change in current after a $\pi(f_2^e)$ pulse (Fig. 2C). In an idealized single-spin system, this would result in a current change on resonance if the nuclear spin was in the $|\downarrow_n\rangle$ (or 0) configuration, and no change in the $|\uparrow_n\rangle$ (1) configuration (*25*). For the ensemble we investigated, we expect a current change after nuclear storage $\Delta I^\tau \propto \alpha^2 \Delta I$ determined by the rotation angle, where $\Delta I$ is the transient if there is no storage (Fig. 2B) or if the logical value 0 is stored (no preparation pulse). If the pulses applied to the system resulted in perfect π rotations of the electron and nuclear spins, we would expect $\Delta I^\tau = 0$; however, imperfections in the pulse duration and homogeneity, the incomplete electron spin polarization, and the inhomogeneous linewidth of the nuclear resonance all reduce the fidelity of our CNOT implementation, and thus some of the spins are not ideally stored. The transient current is therefore not completely eliminated (Fig. 2D) but is reduced as compared to the no-storage case (Fig. 2E). The system can be reset by applying a long pulse at $f_2^n$.

To confirm that the signal in Fig. 2E is due to storage in the phosphorus nuclear spin, we repeated the STORE-1 sequence while varying the frequency of the storage pulse. Figure 3A shows the boxcar-averaged change in $\Delta I$ after the readout pulse after storage for 10 ms. A resonance is clearly seen at 89.1 MHz, corresponding to the $f_1^n$ transition. The resonance is a positive change in the current transient, corresponding to fewer electronic spins being excited during the readout pulse.

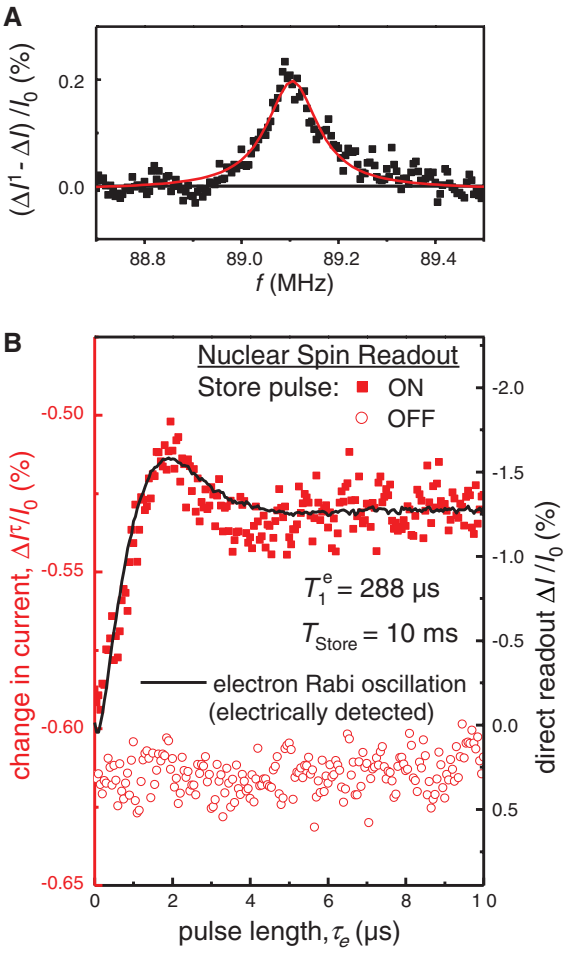


**Fig. 3.** (**A**) Applying the STORE-1 sequence, nuclear storage occurs only when the applied rf radiation is resonant with the $f_1^n$ transition (Lorentzian fit). f, frequency. (**B**) By varying the length of the electron preparation pulse, an arbitrary electron spin state can be stored in the nuclear spin ensemble. The black line shows the prepared electronic spin state readout immediately after preparation (a single-pulse Rabi experiment, right axis), and the square red data points show the read from the nuclear spins after 10 ms of storage (the STORE-τ sequence for varying $\tau_e$) (left axis). With no storage, the initial spin information is lost (open red circles).

Figure 3B shows an electron spin Rabi oscillation (black line), electrically detected immediately after a preparation pulse, $\tau_e(f_2^e)$. The oscillations, while visible, are damped with a Gaussian envelope of width 1.7 μs, due to spatial inhomogeneities in the oscillating magnetic field of the microwaves used to drive the electron spin resonance. By using a STORE-τ sequence, we are able to write an arbitrary electron state to the nuclear memory, store it there, and then use a read pulse to obtain the state from memory $T_{Store}$ = 10 ms later (solid red squares, Fig. 3B). To confirm that the information is indeed stored in the nuclear spins, the experiment was repeated with no storage pulse (open red circles) and with a nonresonant storage pulse (not shown in Fig. 3B); in neither case is the initial electron state recovered. It is important to note that it is not the coherent electron state prepared by the initial pulse but the projection of this state onto the spin eigenstates (the coefficients α and β) that we are storing in the nuclear spin polarization. Including a $\pi(f_2^e)$ pulse after the store pulse would allow a coherent state to be stored and subsequently read out electrically. We expect, however, that such a stored state would decohere within $T_2^n \leq 2T_1^e = 576$ μs (*2*).

To determine the time scale on which the electron spin state can be stored in the nuclear spin, we stored a spin state, in this case 1, and watched its relaxation back to the steady state. Figure 4A shows the result of repeated storage and readout of the electron spin state 1. In Fig. 4B, the storage pulse is moved off resonance, and the nuclear spin memory slowly relaxes back to the initial 0 state with a time constant $T_{Store} = 112 \pm 2$ s. This is close to the 150 ± 20 s Overhauser relaxation rate (electron-nuclear spin flip-flops) previously seen in Si:P under illumination in similar high magnetic field conditions (*15*). We have thus been able to increase the spin storage time by a factor >3 × $10^5$ as compared to $T_1^e$. By varying the experimental conditions, even longer storage times may be accessible: Nuclear spin lifetimes exceeding 10 hours at magnetic fields of around 0.3 T have been observed with conventional ENDOR experiments (*3*).

After relaxation, the store pulse frequency is moved back into resonance (Fig. 4C), and the signal returns to the value associated with storing a 1. A small number of repetitions are required to return to the 1 state because of the imperfect π rotations used in this experiment, and are not an intrinsic feature of this scheme. Figure 4, D and

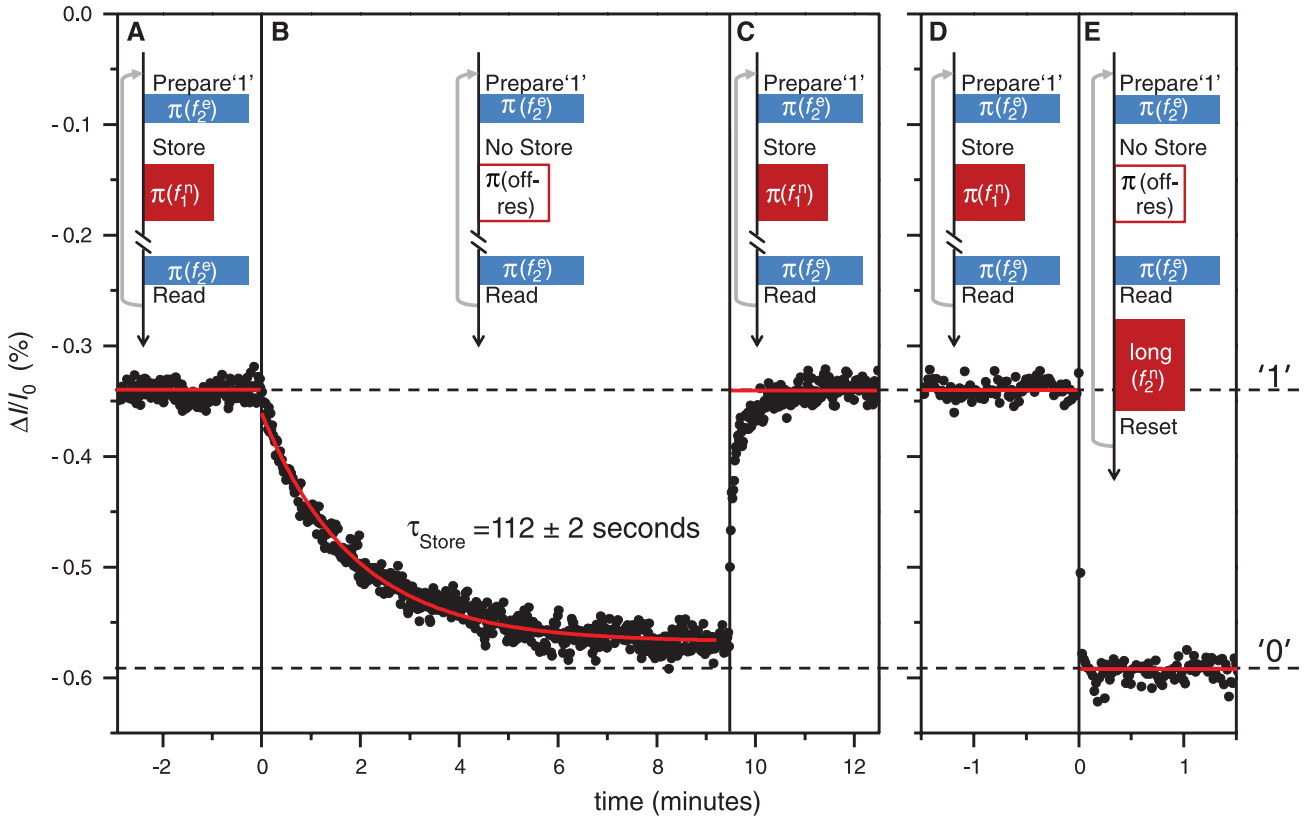


**Fig. 4.** (**A**) Repetitive application of STORE-1 (without a reset pulse) demonstrates the stability of the stored nuclear information ($T_{Store}$ = 10 ms). (**B**) At $t$ = 0, the frequency of the store pulse is detuned from the resonance by 300 kHz (from 89.1 to 88.8 MHz), and the stored information is repetitively read out. The stored spin state is lost from memory with an exponential time constant of 112 ± 2 s. (**C**) At $t \approx 9.5$ min, the store pulse is returned to the resonant frequency, and the 1 state is seen again. The nonzero recovery time of the stored state is due to the imperfection of the applied storage pulses. (**D**) To demonstrate the effectiveness of resetting the memory, a STORE-1 pulse without reset was applied. (**E**) At $t$ = 0, the store pulse frequency was again moved off resonance and the reset pulse turned on. The read state quickly returned to the 0 state.

E, show a similar experiment: In Fig. 4D, a 1 is repetitively prepared, stored, and read out. The store pulse is again moved off resonance, but now a reset pulse is introduced (Fig. 4E); as can be seen, the stored signal is immediately destroyed, and the initial 0 state is recovered.

As well as allowing a measure of the storage lifetime, Fig. 4, B and D, reveal another advantage of the storage method demonstrated here: repetitive readout of the stored spin state (*6*, *25*). Most readout techniques for obtaining the spin state of a donor electron require that the state be destroyed (*13*, *14*, *18*, *26*). Here, however, we have shown that the electron spin state can be stored in the nuclear spins and that the state of the nuclear spin can then be repetitively read out without changing the state. We have measured the stored spin over 2000 times without any observable impact on its state (*27*).

The phosphorus nuclear spin is not the only relevant nucleus for the electrical readout approach demonstrated here. The storage and readout scheme described above was performed on natural silicon containing ~5% spin ½ $^{29}$Si (fig. S1). As the hyperfine coupling between $^{29}$Si nuclei and the $^{31}$P donor electron varies depending on the relative position, an addressable nuclear spin register for the storage of multiple electron spin states in different $^{29}$Si nuclear spins is obtained. $^{29}$Si nuclear spins have extremely long lifetimes (*28*), making them another promising storage system. Donors such as Bi may also be amenable to such a scheme (*16*, *17*). Indeed, the approach presented here may have wide application in spectroscopic investigations of small-scale nuclear spin systems, where conventionally detected approaches are inapplicable.

It is possible to store logical information from donor electronic spins in donor nuclear spins for times exceeding 100 s. Previous work on phosphorus in silicon has demonstrated spin-conserved transport of polarized conduction electrons over long distances (*11*), local spin resonance on the micrometer scale (*29*), electrical detection of the spin resonance signal from as few as 50 donors (*26*), and single-shot detection of the state of a single spin (*14*). Combining these advances should enable the development of a practical spin memory in silicon, possibly at the single donor level.

### References and Notes


1. W. M. Witzel, S. Das Sarma, *Phys. Rev. B* **76**, 045218 (2007).
2. J. J. L. Morton *et al.*, *Nature* **455**, 1085 (2008).
3. G. Feher, E. A. Gere, *Phys. Rev.* **114**, 1245 (1959).
4. L. Childress *et al.*, *Science* **314**, 281 (2006).
5. L. Jiang *et al.*, *Science* **326**, 267 (2009).
6. P. Neumann *et al.*, *Science* **329**, 542 (2010).
7. B. Stich, S. Greulich-Weber, J.-M. Spaeth, *Appl. Phys. Lett.* **68**, 1102 (1996).
8. G. Yusa, K. Muraki, K. Takashina, K. Hashimoto, Y. Hirayama, *Nature* **434**, 1001 (2005).
9. M. Fuechsle *et al.*, *Nat. Nanotechnol.* **5**, 502 (2010).
10. S. P. Dash, S. Sharma, R. S. Patel, M. P. de Jong, R. Jansen, *Nature* **462**, 491 (2009).
11. I. Appelbaum, B. Huang, D. J. Monsma, *Nature* **447**, 295 (2007).
12. A. Tyryshkin, S. Lyon, A. V. Astashkin, A. M. Raitsimring, *Phys. Rev. B* **68**, 193207 (2003).
13. B. E. Kane, *Nature* **393**, 133 (1998).
14. A. Morello *et al.*, *Nature* **467**, 687 (2010).
15. D. R. McCamey, J. van Tol, G. W. Morley, C. Boehme, *Phys. Rev. Lett.* **102**, 027601 (2009).
16. R. E. George *et al.*, *Phys. Rev. Lett.* **105**, 067601 (2010).
17. G. W. Morley *et al.*, *Nat. Mater.* **9**, 725 (2010).
18. G. W. Morley *et al.*, *Phys. Rev. Lett.* **101**, 207602 (2008).
19. J. van Tol, L.-C. Brunel, R. J. Wylde, *Rev. Sci. Instrum.* **76**, 074101 (2005).
20. G. W. Morley, L.-C. Brunel, J. van Tol, *Rev. Sci. Instrum.* **79**, 064703 (2008).
21. Supporting material on *Science* Online includes experimental methods and additional data.
22. A. M. Tyryshkin, J. J. L. Morton, A. Ardavan, S. A. Lyon, *J. Chem. Phys.* **124**, 234508 (2006).
23. G. W. Morley *et al.*, *Phys. Rev. Lett.* **98**, 220501 (2007).
24. J. J. L. Morton, N. S. Lees, B. M. Hoffman, S. Stoll, *J. Magn. Reson.* **191**, 315 (2008).
25. M. Sarovar, K. C. Young, T. Schenkel, K. B. Whaley, *Phys. Rev. B* **78**, 245302 (2008).
26. D. R. McCamey *et al.*, *Appl. Phys. Lett.* **89**, 182115 (2006).

27. The state 1 varied during nondemolition readout due to the intrinsic relaxation toward the steady state 0. No change was observed in the 0 state.
28. T. D. Ladd, D. Maryenko, Y. Yamamoto, E. Abe, K. M. Itoh, *Phys. Rev. B* **71**, 014401 (2005).
29. L. H. Willems van Beveren *et al*., *Appl. Phys. Lett.* **93**, 072102 (2008).
30. This work was supported in part by Visiting Scientist Program Grant 12488 from the National High Magnetic Field Laboratory (NHMFL). The NHMFL is funded by the State of Florida, the U.S. Department of Energy, and NSF through Cooperative Agreement DMR-0654118. D.R.M. acknowledges support through an Australian Research Council Postdoctoral Fellowship (DP1093526). G.W.M. acknowledges support from the Royal Commission for the Exhibition of 1851 and the EPSRC COMPASSS grant. C.B. acknowledges support from the NSF CAREER program (grant 953225).

**Supporting Online Material**
www.sciencemag.org/cgi/content/full/330/6011/1652/DC1
Materials and Methods
Figs. S1 to S3
References

17 September 2010; accepted 9 November 2010
10.1126/science.1197931

# Oxygen Doping Modifies Near-Infrared Band Gaps in Fluorescent Single-Walled Carbon Nanotubes

**Saunab Ghosh,[1] Sergei M. Bachilo,[1] Rebecca A. Simonette,[2] Kathleen M. Beckingham,[2] R. Bruce Weisman[1]***

**Controlled chemical modifications of single-walled carbon nanotubes (SWCNTs) that tune their useful properties have been sought for multiple applications. We found that beneficial optical changes in SWCNTs resulted from introducing low concentrations of oxygen atoms. Stable covalently oxygen-doped nanotubes were prepared by exposure to ozone and then light. Treated samples showed distinct, structure-specific near-infrared fluorescence at wavelengths 10 to 15% longer than displayed by pristine semiconducting SWCNTs. Dopant sites harvest light energy absorbed in undoped nanotube regions by trapping mobile excitons. The oxygen-doped SWCNTs are much easier to detect and image than pristine SWCNTs because they give stronger near-infrared emission and do not absorb at the shifted emission wavelength.**

One of the most remarkable characteristics of single-walled carbon nanotubes (SWCNTs) is their diversity of well-defined electronic and optical properties (*1*, *2*). Each SWCNT is composed of covalently bonded carbon atoms forming an ordered tubular structure with a specific diameter and roll-up angle, uniquely defined by a pair of integers called the (*n*,*m*) index. About two-thirds of SWCNT structures are semiconducting. Their intrinsic band gaps are determined by quantum confinement and linked to physical structure, with only slight alterations possible through environmental perturbation.

A variety of optical and electronic applications would benefit from the controlled modification of SWCNT band gaps in bulk samples, individual nanotubes, and even segments within nanotubes. Covalent sidewall reactions have been used to bond nanotubes to chemical groups having a range of selected electronic properties (*3*, *4*). However, to date such reactions have randomly eroded the highly ordered nanotube π-electron structure. The additional covalent bonds remove electrons from the π-system, broadening and suppressing the signature near-infrared (IR) fluorescence peaks of semiconducting SWCNTs (*5*). Here, we describe a different type of chemically modified SWCNT that is more analogous to dopant-tuned semiconductor materials. These stable and easily prepared oxygen-doped nanotubes are near-IR fluorophores that display distinct, structure-specific optical properties systematically shifted from those of the pristine parent. They are more readily detected than pristine nanotubes.

We produce these modified SWCNTs by exposing aqueous suspensions of pristine SWCNTs to low doses of ozone and then photolyzing the resulting product (*6*). Our studies rely on samples highly enriched in individual semiconducting (*n*,*m*) species through nonlinear density gradient ultracentrifugation (*7*). The simpler optical spectra of these sorted samples allow monitoring of the conversion reaction by fluorescence spectroscopy. Immediately after mild ozone exposure, the characteristic near-IR $E_{11}$ fluorescence band shows small red shifts (~0.2) and appreciable broadening (~5%). Subsequent exposure to light induces a new emission feature, termed $E_{11}$*, that is red-shifted from $E_{11}$. Spectra measured during this transformation are shown for a (6,5)-enriched sample in Fig. 1A. During phototransformation by light from a desk lamp, 980-nm $E_{11}$ emission diminishes as the 1120-nm $E_{11}$* feature increases (Fig. 1, A and B). However, except for some broadening, the absorption spectrum remains essentially unchanged by this conversion (Fig. 1C). The transformed nanotubes show very little absorption at their new emission peak, unlike pristine SWCNTs. We estimate that the photoconversion efficiency is quite low, requiring $10^7$ to $10^9$ absorbed photons per micrometer of SWCNT length. An excitation-emission contour plot demonstrates that near-IR emission from both the original and the transformed (6,5) sample is induced by absorption at the same $E_{22}$ transition (Fig. 1D). The shifted emission from our converted SWCNTs differs in wavelength from the weak intrinsic satellite features observed in pristine samples (*8*–*10*). In addition to the prominent shifted emission band, a weak secondary shifted feature can also be seen (*6*).

Very low ozone doses followed by photoconversion are required to prepare such modified SWCNTs. They are qualitatively different from those prepared through more extensive nanotube ozonation (*11*–*17*), which quenches SWCNT near-IR fluorescence (*18*). Of several ionic surfactants used to suspend samples during ozonation treatment, we found that sodium tridecylbenzenesulfonate (STBS) gave the most reproducible results, presumably because it could be used at lower concentrations that compete less for reaction with ozone. Resonance Raman spectra revealed that the ozone-and-photolysis transformation was accompanied by the appearance of a sharp D-band near 1310 $cm^{-1}$ (figs. S10 and S11) signifying covalent functionalization of the nanotube sidewall (*19*). The transformation reaction also occurred, although less efficiently, when weaker oxidants $H_2O_2$ or $K_2CrO_4$ were substituted for ozone (fig. S18) (*6*). We conclude that the transformed nanotubes incorporate covalently bonded oxygen. Similar but unintended oxidation may have led to the defect-induced emission reported from some individual SWCNTs exposed to intense pulsed laser light (*20*).

Other semiconducting (*n*,*m*) species also underwent oxygen doping. For example, bulk samples enriched in (6,4) and (8,3) showed reduced $E_{11}$ emission and the growth of a new red-shifted $E_{11}$* emission band as they were treated with ozone and visible light (fig. S9). Spectral transformations were less efficient for larger-diameter SWCNTs (fig. S15) (*6*). We measured spectral positions and widths of $E_{11}$* peaks from 10 different oxygen-doped (*n*,*m*) species in STBS for comparison with their pristine forms (Table 1). The spectral red shifts between $E_{11}$ and $E_{11}$* ranged from 106 to 214 meV and showed a strong positive correlation with $E_{11}$ (Fig. 1E) (*21*). These doping-induced shifts represent optical band gap decreases of 10 to 15% from the pristine values.

Spectroscopic measurements on individual nanotubes revealed photophysical heterogeneity in the doped samples. The results are illustrated with fluorescence spectra acquired from three individual nanotubes in a (6,5)-enriched bulk sample (Fig. 2A). One nanotube was pristine and

[1]Department of Chemistry and R. E. Smalley Institute for Nanoscale Science and Technology, Rice University, Houston, TX 77005, USA. [2]Department of Biochemistry and Cell Biology and R. E. Smalley Institute for Nanoscale Science and Technology, Rice University, Houston, TX 77005, USA.

*To whom correspondence should be addressed. E-mail: weisman@rice.edu